UNIVERSITÀ DEGLI STUDI DI BERGAMO
DIPARTIMENTO DI INGEGNERIA DELL'INFORMAZIONE
E METODI MATEMATICI°

QUADERNI DEL DIPARTIMENTO

Department of Information Technology and Mathematical Methods

Working Paper

Series "*Mathematics and Statistics*"

n. 4/MS – 2009

A method for studying dental crown and apex position statistics

by

G. Mannarini, C. Mannarini, A. Fassò

° Viale Marconi. 5, I – 24044 Dalmine (BG), ITALY, Tel. +39-035-2052339; Fax. +39-035-562779

[§] L'accesso alle *Series* è approvato dal Comitato di Redazione. I *Working Papers* della Collana dei Quaderni del Dipartimento di Ingegneria dell'Informazione e Metodi Matematici costituiscono un servizio atto a fornire la tempestiva divulgazione dei risultati dell'attività di ricerca, siano essi in forma provvisoria o definitiva.

A method for studying dental crown and apex position statistics

Gianandrea Mannarini

Dept. of Electronics for Automation, University of Brescia (Italy)
Address: via Branze 38, I-25123 Brescia
Phone: +39-030-3715510; Fax: +39-030-380014
Email: Gianandrea(DOT)Mannarini(AT)ing(DOT)unibs(DOT)it

Carolina Mannarini

Dept. of Orthodontics, University of Ferrara (Italy) and private practice in Lecce (Italy)

Alessandro Fassò

Dept. of Information Technology and Mathematical Methods, University of Bergamo (Italy)

Abstract

Human dental arch shape and arch shape variability are investigated using Computed Tomography pictures of 62 patients. Both crown level and radicular apex level data are considered. For each patients, four axial sections parallel to the occlusal plane are selected, in order to be representative of crown and apex part of the dental arches, both in the maxilla and the mandible. Tooth landmarks are located on each of these planes. After standardization of landmark positions, it is seen that landmarks relative to a given tooth cluster into "'subclouds"'. Tranforming datapoints into polar coordinates, it is possible to approximtely follow mesio-distal and bucco-lingual directions. It is found that in a direction close to the mesio-distal one, crown subclouds are (for most teeth) significantly narrower than apex subclouds. This is possibly a manifestation of interproximal contact at crown level.

Keywords: dental root apex, computed tomography, arch form, interproximal contact.

April 6, 2009

1 Introduction

Human dental arch shape has been an open research field for at least one century. Attempts to define an arch shape have sometimes resorted to the field of normal anatomy: The existence of a reference, "normal" shape of the dental arch was postulated, which has got the feature of being in harmonic equilibrium with the dental bone as well as with the surrounding musculature [13, 11]. At the beginnings, not only the mere existence but even the actual shape of such a normal dental arch was postulated. Reminiscences of classical canons of beauty and harmony, such as the equilateral triangle and the circle, appear in the first geometrical models of dental arch form [4]. With the advent of computers' era, arch forms of increasing mathematical complexity have been tested for a more accurate description of human dental arch. There has been many different ideas about how to place landmarks on teeth [10, 3, 6], and what kind of mathematical functions to be used [8, 1, 2]. There was a work by Sampson [10] which asks the quantitative question: How far is an actual arch form from the most frequent arch form (in an observed population)? The answer was given in the frame of a statistical theory for the distribution of arch forms (the theory was restricted to conic sections).

Existing published literature on dental arch form concerns, to the best of our present knowledge, with crown dental data only. The landmarks were placed on either maxilla or mandible teeth after casts were photographed [8, 3, 1, 6] or optically scanned [9]. In any case, information about only the visibly accessible part of the tooth was employed. Computed Tomography (CT) however, using X-radiation, allows to access also the internal part of the anatomic structures. In particular, cone beam CT has been recently introduced for the study of the maxillo-facial region [7]. Using CT data, we are able to treat dental crown and apex landmark arches on the same footing for the first time. We employ this information for comparing the statistical fluctuations of arch shape. The question arises, if such fluctuations are larger at crown or apex level. Also, the components of such fluctuations along bucco-lingual (BL) and mesio-distal (MD) direction are of interest.

The present research would like to address the question of the variability of dental crown and apex positions among members of a statistical ensemble. To this end, we propose to describe the whole set of landmarks in a system of polar coordinates. It will be shown that such frame allows a more natural description of the dental system than what possible in cartesian coordinates. Staying in the polar frame, we compare the variability of tooth landmarks at crown and apex level by statistical tests of the ratio of the variances (F-tests). Furthermore, a relatively simple description of arch shape, both at crown and apex level, is derived as a by-product of our method.

The heart of this paper is the "Material and Methods" section. Since we refrain from an abstract presentation of the method, it is unavoidable that in this section the main results are presented along with the method itself. However, we review and deepen the findings in the "Results" section. We discuss critically our work in the "Discussion" section. Finally, we draw our conclusions, which contain a brief summary of the main results and their interpretation.

2 Material and Methods

The method of investigation developed in this work consists into two major parts: The first part is data collection and selection; the second part is mathematical processing of data.

2.1 Data collection and selection

CT data of human cranial region are collected from radiological centers and private practices across Italy, as listed in the Acknowledgments section.

A subset of these CTs has been selected on the basis of the following criteria: i) presence of one or two dental arches, including all teeth from central incisors to first molars; ii) absence of any conservative or prosthetic reconstructions. After application of the selection criteria i) and ii), data from 62 patients were retained (details of the the dataset can be found in Tab. 1). Part of these CTs has been produced by means of the Newtom 3G cone beam digital volumetric tomograph (QR s.r.l., Verona, Italy) and part by means of the General Electric CT/E Dual digital volumetric tomograph (General Electric, USA).

For each one of the 62 patients, we have reconstructed axial sections using the tomograph software. The sections have been taken to be parallel to the occlusal plane. This is achieved by rotating the analysis volume of the tomography along one or two orthogonal axes, as shown in Fig. 1. We have considered two couples of axial sections: Crown sections and apex sections, for both maxilla and mandible. Crown sections are defined by the contact point of latero-posterior teeth; apex sections are taken within the third apical of the dental roots, Fig. 1. Typical axial sections obtained this way are displayed in Fig. 2.

Once the axial sections are chosen, representative landmarks for each dental element are located. For crowns, landmarks are placed at the center of the segment connecting interproximal contact points. For apexes, landmarks are placed at the root center for monoradicular teeth; at the center of the line through the two roots for biradicular teeth; at the barycenter of the triangle with vertex at the roots for triradicular teeth, Fig. 2. The landmarks are positioned on top of the image of the axial section using OpenOffice Impress (Sun Microsystems Inc., USA). The same software makes possible to digitize the position of the landmarks by reading out their x and y coordinates on the axial section plane. Previously to this, the image of the axial section together with its landmarks is rotated in the $x - y$ plane for ensuring that the y coordinates of the first molars are identical. For each patient, using OpenOffice Calc (Sun Microsystems Inc., USA), a datasheet is produced containing the coordinates of all available dental elements. Complete dental arches only are considered, since absence of one or more teeth might have led to a spatial reorganization of the positions of the dental elements.

2.2 Data processing

The full set of patient datasheets is read out and processed by a software in the IGOR Environment (WaveMetrics Inc., Oregon, USA), designed and written by the first author of this paper. Before proceeding with the description of the processing method, it is necessary to enlarge the existing nomenclature. From now on, we refer to the set of landmarks placed on either a crown or an apex section by the phrase "landmark arch" or $\mathcal{L}$-arch. Thus, each dental arch comprises an apex $\mathcal{L}$-arch and a crown $\mathcal{L}$-arch. A plot

	crown_up	apex_up	crown_dn	apex_dn
# complete $\mathcal{L}$-arches	32	35	43	45
# complete dental arches	29		39	
# complete both jaws	16			

Table 1: *Summary table of the patient database size.*

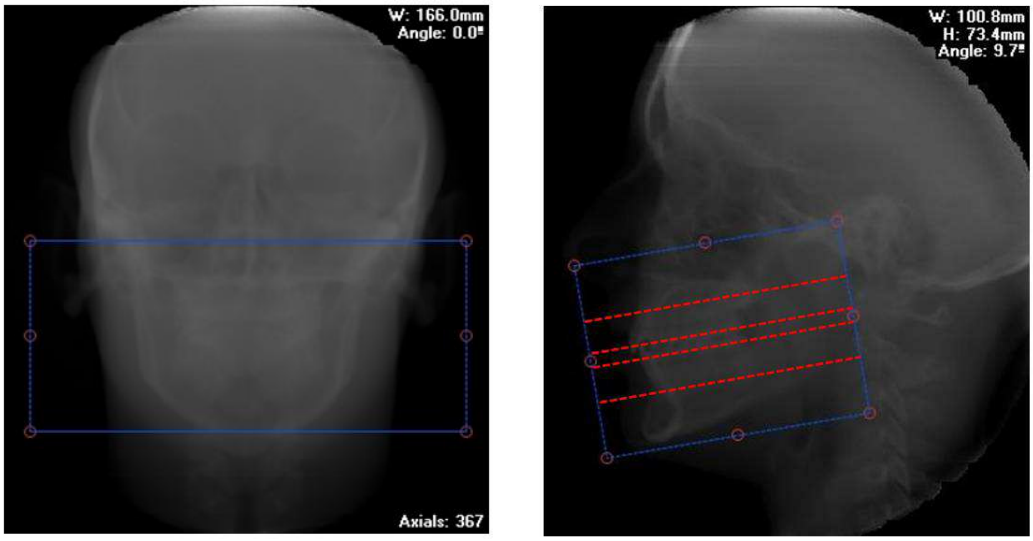

Figure 1: *Example of sagittal sections showing the projections of the subvolumes (blue boxes) chosen for the subsequent analysis. Left and right panel represent frontal (subvolume tilting angle = 0°) and lateral (subvolume tilting angle = 9.7°) view respectively of the same patient. In the right panel, the position of the selected assial sections is also displayed (red dashed lines): From top to bottom they refer to the following $\mathcal{L}$-arches: Maxilla apex; maxilla crown; mandible crown; mandible apex.*

of the four $\mathcal{L}$-arches for the whole patient ensemble is given in Fig. 3. For each $\mathcal{L}$-arch, this leads to a cloud-like representation, since the landmarks belong to dental arches of different size and shape. Furthermore, the landmarks relative to different patients can happen to be freely displaced in the $x-y$ plane, since alignment of the images of the axial sections was not required. Thus, mean $\mathcal{L}$-arch shape can not be directly inferred from this kind of plot.

2.2.1 Standardization of coordinates

For quantitative comparison of landmarks from different patients, we introduce a standardization procedure of the tooth coordinates defined by the following equations:

$$\begin{cases} \xi &= -\frac{1}{2} + \frac{x - x_{l6}}{x_{r6} - x_{l6}} \\ \eta &= \frac{y - y_{l6}}{x_{r6} - x_{l6}} \end{cases} \tag{1}$$

In Eq. (1) the subscript $l(r)$ indicates the left(right) hemiarch of the $\mathcal{L}$-arch which the (x, y) pair belongs to. The transformation defined by Eq. (1) has the property that the first molars ($l6$ and $r6$) are represented by fixed points of coordinates $(\xi, \eta) = (\pm 1/2, 0)$. That is, this transformation corresponds to shifting and rescaling $\mathcal{L}$-arch coordinates in such a way that the first molars of different patients are superimposed. The mutual distance of the first molars is the unit length in the $\xi - \eta$ plane of standardized coordinates. The line connecting the two fixed points is called "baseline" and the (ξ, η) pair represents the shape coordinates. This procedure belongs to the more general family of methods called "landmark registration". For an overview we refer to Bookstein's work [5].

The results of application of transformation Eq. (1) to the datapoints of Fig. 3 are displayed in Fig. 4. There is a striking difference with respect to the plot of the row data. The landmarks tend to cluster into "subclouds", each subcloud corresponding to a

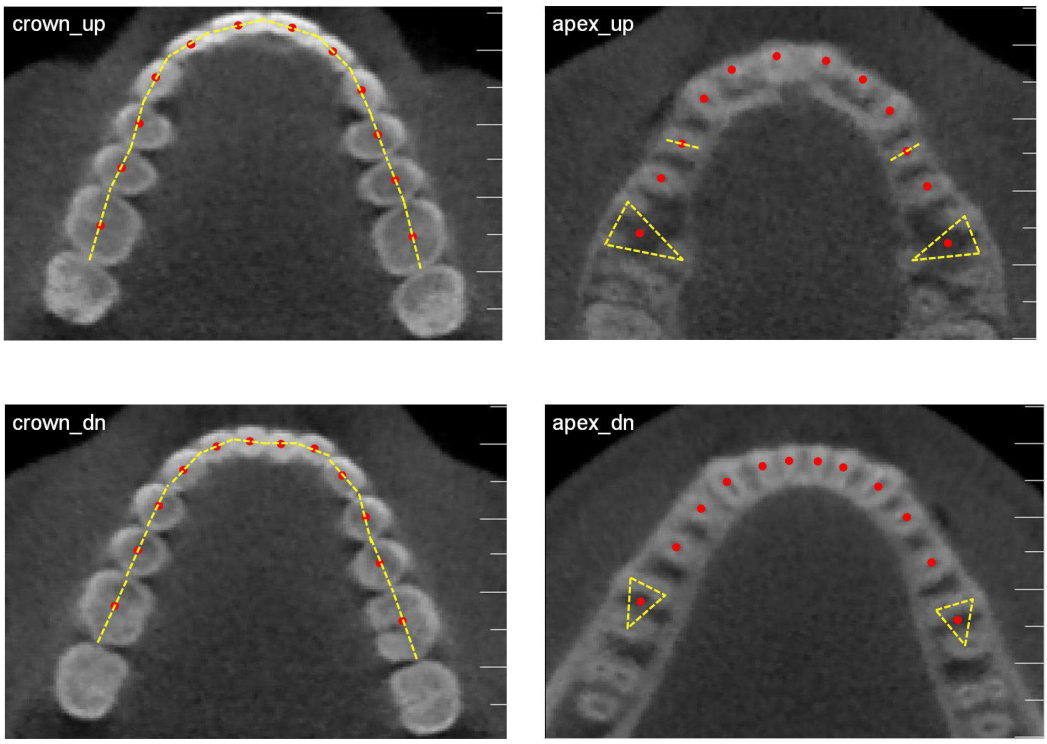

Figure 2: *Assial sections corresponding to the right panel of Fig. 1 with landmarks (red dots) selected to be representative of the dental elements. Left(right) panels display crown(apex) data. Upper(lower) panels display maxilla(mandible) $\mathcal{L}$-arch data. On crown sections, yellow dashed lines connect the interproximal contact points; on apex sections, yellow dashed lines connect the apexes of multi-radicular teeth.*

given tooth (e.g., left central incisor subcloud, right first premolar subcloud, etc.). The clustering is more evident for crown than apex $\mathcal{L}$-arches and for maxilla rather than for mandible data. Furthermore, it is recognized that most of the subclouds are elongated in BL direction. Again, this is clearer for crown $\mathcal{L}$-arches. We have computed point estimates of mean and standard deviation of the coordinates of each subcloud. These statistical indicators are displayed as black markers with error bars in Fig. 4. These markers form what we might call "mean $\mathcal{L}$-arch shape". It is seen from Fig. 4 that, for the case of apex $\mathcal{L}$-arches, such mean shape is quite similar to a hemicircumference. In the case of crowns instead, the mean shape is round in the anterior part and straight in the latero-posterior region; The change of curvature can be recognized to occur in the vicinity of the canine tooth.

2.2.2 Polar coordinate representation

The observations made about $\mathcal{L}$-arch shape and subcloud structure after application of the standardization procedure Eq. (1) suggest us to describe $\mathcal{L}$-arches in another reference frame. Indeed, in Fig. 4 the coordinate variability of most dental element is described by two bars (i.e., along ξ and η) of comparable size. However, given the elongation of the subclouds, it seems to us more natural to look at the data in a frame in which the variability along BL and MD direction can be more easily distinguished. This means giving up on the rectangular frame in favor, for instance, of a polar one. Thus, we

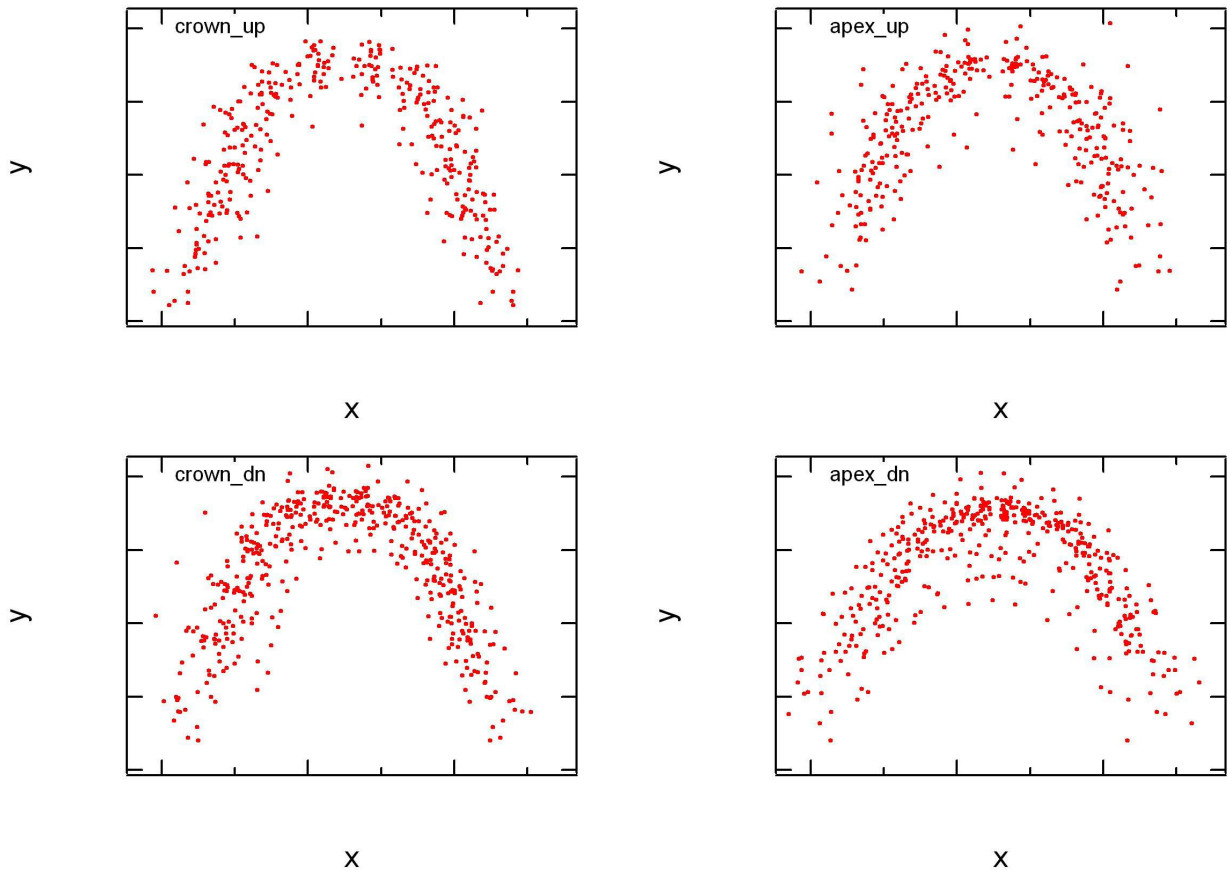

Figure 3: *Tooth landmarks of the whole patient ensemble. Left(right) panels display crown(apex) data. Upper(lower) panels display maxilla(mandible) $\mathcal{L}$-arch data.*

consider a new coordinate transformation, defined by

$$\begin{cases} \rho &= \sqrt{\xi^2 + \eta^2} \\ \theta &= \dfrac{180}{\pi}\left(\dfrac{\pi}{2} - \arctan(\eta/\xi)\right) \end{cases} \tag{2}$$

The new coordinate ρ is the distance from the origin $(\xi = 0, \eta = 0)$ of the $\xi - \eta$ plane, measured in units of the distance between first molars. For a perfectly circular $\mathcal{L}$-arch (dashed line in Fig. 4), the ρ axis would coincide with the BL direction. The θ angle (in degrees) is measured from the η (vertical) axis and increases from the negative to the positive ξ (horizontal) axis. For a perfectly circular $\mathcal{L}$-arch, an infinitesimal increase in θ direction would coincide with the MD direction.

The polar coordinate representation of data in Fig. 4 is displayed in Fig. 5. The observation that most crown subclouds are elongated in BL direction is strongly supported by this representation. The subclouds are nearly vertically aligned in the polar representation: Most of the landmarks relative to a given tooth are found at nearly the same angular coordinate θ. For apexes, the situation is less defined and, especially in the mandible, the subclouds can partially merge into another.

2.2.3 Variability of the $\mathcal{L}$-arch elements position

We have already observed that the subcloud narrowing along MD direction seems to be more evident for crown than for apex $\mathcal{L}$-arches Fig. 4, while it is not clear, even from Fig. 5, what the crown-to-apex ratio of subcloud sizes along BL direction is. We wish

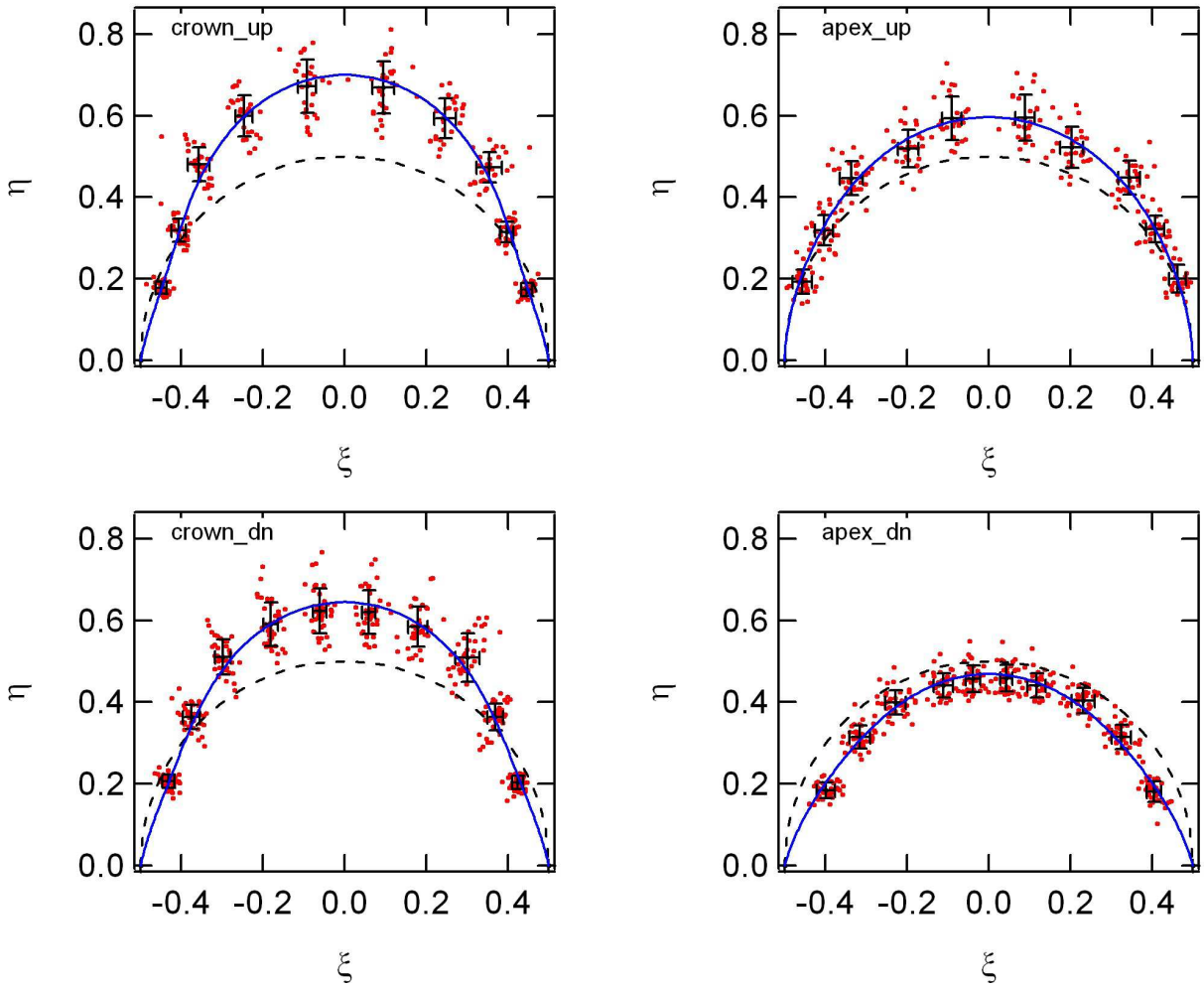

Figure 4: *Rescaled tooth landmark positions according to Eq. (1). The black markers are centered at the mean (rescaled) coordinates of each tooth and the halfwidth of their error bars is one standard deviation of the tooth (rescaled) coordinate variability. The black dashed curves are the hemicircumferences of unit diameter passing through the fixed points* $(\pm 1/2, 0)$*. The blue solid curves are least square fits to the mean dental positions, according to Eq. (5) and back transformed into rectangular coordinates using the inverse of the transformation defined by Eq. (2).*

now to investigate these size ratios more quantitatively. Thus, we make a statistics of the deviations of the landmarks from their mean positions. In the following, we call such deviations "statistical errors". Staying in the polar frame, the errors $\omega_{a,t,p}$ and the errors $\epsilon_{a,t,p}$ for $\mathcal{L}$-arch a, tooth t, and patient p are defined as:

$$\begin{aligned} \omega_{a,t,p} &= \theta_{a,t,p} - \overline{\theta_{a,t}} \\ \epsilon_{a,t,p} &= \rho_{a,t,p} - \overline{\rho_{a,t}} \\ & a = 1..4 \quad t = -5..-1, 1..5 \quad p = 1..n = 62 \end{aligned} \tag{3}$$

(The overline denotes the subcloud mean value). First, we compute the distribution of the errors (we restrict to 10 dental elements per $\mathcal{L}$-arch, since the first molars are fixed points and, thus, do not exhibit a subcloud structure). The Lilliefort test results in statistically significant acceptance of a normal distribution of $\omega_{a,t,p}$ for all but four subclouds along θ, Tab. 2, and in statistically significant acceptance of a normal distribution of $\omega_{a,t,p}$ for all but one subcloud along ρ, Tab. 3.

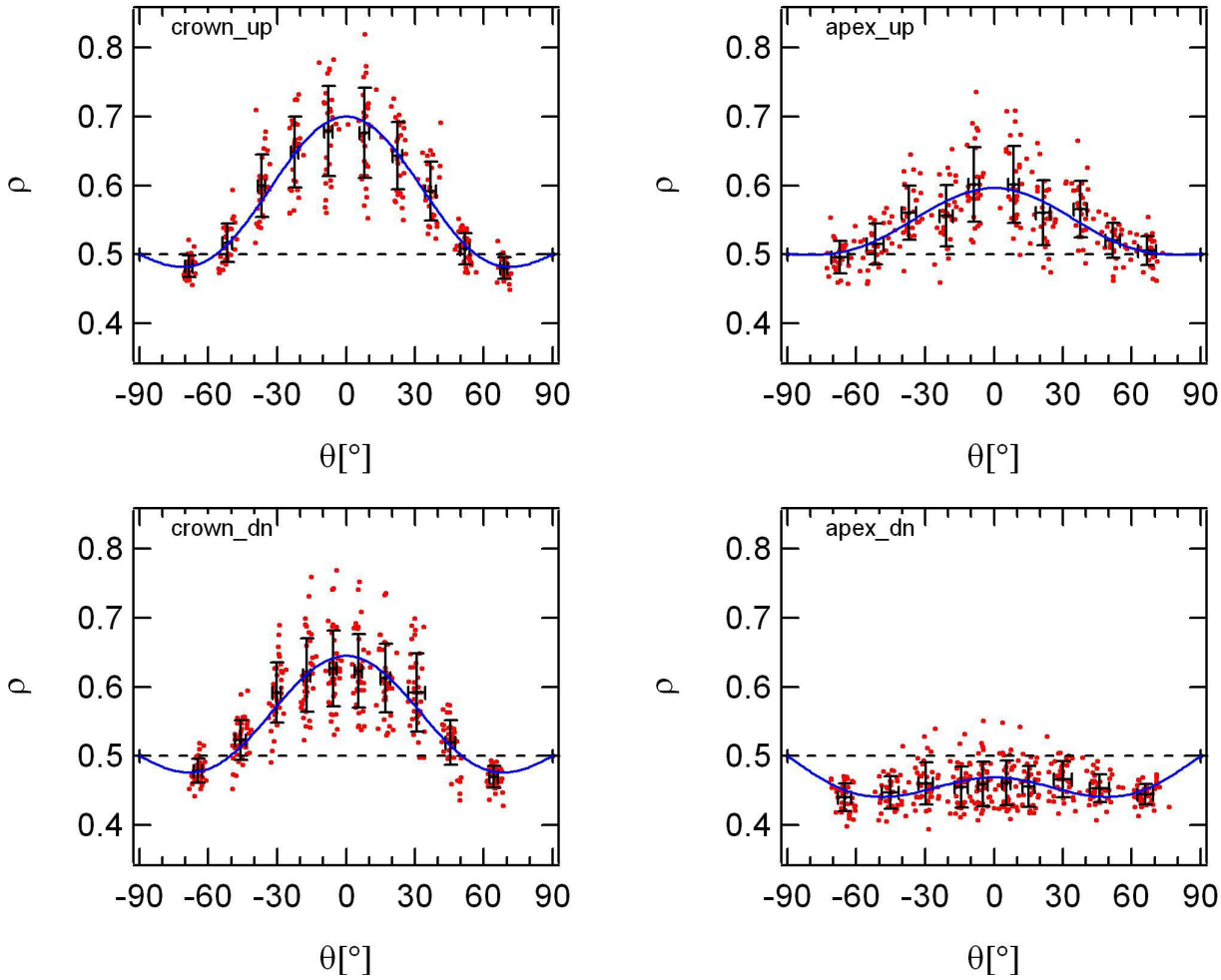

Figure 5: *Polar coordinate representation according to Eq. (2) of the data in Fig. 4. The black markers are centered at the mean (polar rescaled) coordinates of each tooth and the halfwidth of their error bars. The black dashed lines correspond to the hemicircumferences of Fig. 4. The blue solid curves are least square fits to the mean dental positions, according to Eq. (5).*

Then, we test if the ratio of crown to apex subcloud variance is equal to unity. This is the mathematical formulation of the question "are crown subclouds as wide as apex subclouds?". The normality of the distributions tested previously implies in particular that the sample variance S and the variance σ are proportional via an adequate χ^2-distribution (n is the number of complete dental arches, see Tab. 1):

$$S^2 = \sigma^2 \frac{\chi^2_{n-1}}{n-1} \tag{4}$$

Thus, the S_c^2/S_a^2 ratio of crown to apex sample variances follows a $F_{n-1,n-1}$ statistics. All the statistical tests described in this paragraph have been carried out in the R environment (a free software available at http://www.r-project.org/).

2.2.4 Mean shape of the $\mathcal{L}$-arches

The polar representation of Fig. 5 also suggests a way of describing $\mathcal{L}$-arch shape. First, we note that a circular $\mathcal{L}$-arch (the one passing through the first molars) would appear in the polar representation as a straight horizontal line of coordinate $\rho = 1/2$. In real $\mathcal{L}$-arches

$\mathcal{L}$-arch / θ	l5	l4	l3	l2	l1	r1	r2	r3	r4	r5
apex_up	.653	.591	.566	.608	.312	.346	.219	.229	.340	*.013*
crown_up	.678	.274	.982	.951	.185	.037	.523	.867	.981	.899
crown_dn	.479	.882	.919	.074	.812	.860	*.026*	*.001*	.726	.425
apex_dn	.348	.618	.839	.511	*.027*	.800	.160	.772	.172	.265

Table 2: *p-values of the normality tests for the statistical errors $\omega_{a,t,p}$. The subcloud distributions along θ have been analyzed through the Lilliefort test. For each dental element, the null hypothesis corresponds to a normal distribution. The null hypothesis is rejected for $p < .050$. In such case, the p-value is printed in italics.*

$\mathcal{L}$-arch / ρ	l5	l4	l3	l2	l1	r1	r2	r3	r4	r5
apex_up	.693	.331	.481	.697	.054	.234	.457	.664	.669	.945
crown_up	.790	.686	.182	.081	.305	.483	.296	.689	.579	.847
crown_dn	.283	.573	.996	.062	.053	.133	.312	.914	.077	.377
apex_dn	.674	.656	.315	*.048*	.464	.382	.137	.694	.586	.871

Table 3: *p-values of the normality tests for the statistical errors $\epsilon_{a,t,p}$. The subcloud distributions along ρ have been analyzed through the Lilliefort test. For each dental element, the null hypothesis corresponds to a normal distribution. The null hypothesis is rejected for $p < .050$. In such case, the p-value is printed in italics.*

(with the exception of mandible apexes), however, anterior teeth are more distant from the origin ($\xi = 0, \eta = 0$) than first molars (see dashed line in Fig. 4). Furthermore, from the polar representation of crowns, it is easily recognized that, on the average, second premolars are closer to the origin than first molars, Fig. 5. Thus, a good function $\rho_{\text{fit}}(\theta)$ describing $\mathcal{L}$-arch mean shape should account for the following features: i) $\rho_{\text{fit}}(\pm 90^o) = 1/2$; ii) ρ_{fit} decreasing from first molars to second premolars; iii) ρ_{fit} increasing from second premolars to central incisors. Accounting also for the symmetry of the $\mathcal{L}$-arches, these considerations lead us to use the following model (θ in degrees):

$$\rho_{\text{fit}}(\theta) = \frac{1}{2} + \rho_1 \cos\left(\frac{\pi\theta}{180}\right) + \rho_3 \cos\left(\frac{3\pi\theta}{180}\right) \tag{5}$$

The 1/2 addend and the frequencies of the cosine functions are chosen in order to fulfill the boundary condition (i). The cosine function with the larger period ("fundamental harmonic") is always non negative in the considered angular range $-90^o \leq \theta \leq 90^o$. If the parameter $\rho_1 > 0$, this term accounts for the larger distance from the origin of anterior teeth with respect to first molars, in the case of crown $\mathcal{L}$-arches and maxilla apex $\mathcal{L}$-arch. Conversely, $\rho_1 < 0$ for mandible apex $\mathcal{L}$-arch. The cosine function containing the 3 factor oscillates more rapidly than the fundamental harmonic and exhibits knots at $\theta = \pm 30^o$ and $\theta = \pm 90^o$. Thus, it is negative in the two outer angular regions defined by the knot positions: $30^o < |\theta| < 90^o$. This term accounts for the observed fact that the distance from the origin decreases in the region between first molars and second premolars.

We perform numerical fits of Eq. (5) to the mean tooth coordinates accounting for their variability along *both ρ and θ* direction (orthogonal least squares fit). To this end, we employ the ODRPACK95 routine which is available within the IGOR environment. This way, we can further ensure that the results of the fits are invariant under rotation of the reference frame (cp. Sampson's discussion on this issue in [10]).

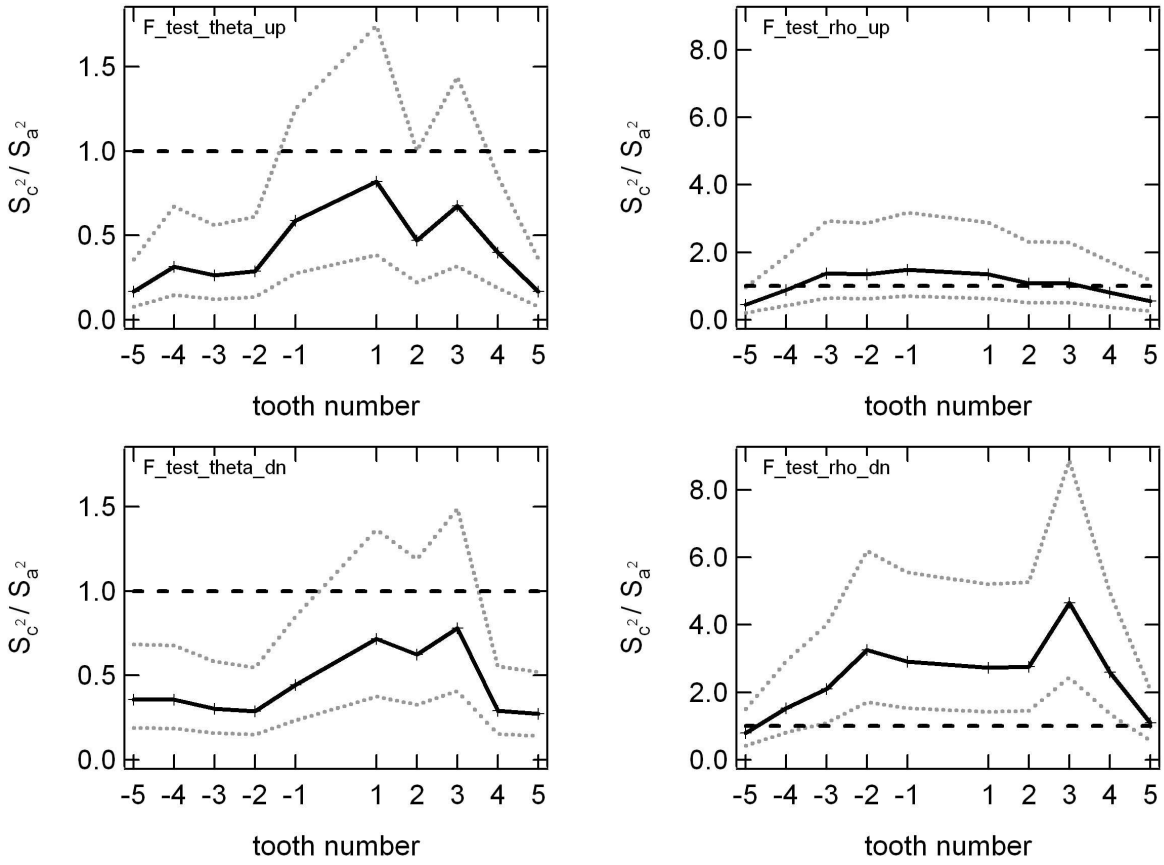

Figure 6: *F-ratio of the variances of the statistical errors for each dental element of both maxilla (top panels) and mandible (bottom panels), plotted each as a solid line. Left(right) panels refer to $\theta(\rho)$ direction. The limits of the 95% confidence interval are plotted as dotted lines. The reference value $F = 1$ is also given (horizontal dashed line).*

3 Results

3.1 Ratio of crown to apex subcloud width

The main results of the application of the outlined method to the 62 patient CT concern the ratio of crown to apex subcloud width and the analysis of the mean shape of the $\mathcal{L}$-arches.

Fig. 5 and the subsequent statistical analysis displayed in Fig. 6 show that, along the θ direction, most crown subclouds are significantly narrower than apex subclouds. This holds for both maxilla and mandible. There are some dental elements in the right hemiarch for which this conclusion does not hold (F-ratio not significantly smaller than unity) but not so in the left hemiarch. Such an asymmetry can be ascribed to still insufficient size of the patient ensemble. However, the crown to apex relative subcloud narrowing along θ seems to be a general feature of our dataset, see Tab. 4. Fig. 6 and Tab. 5 further show that in radial direction instead crown subclouds are either nearly as large as apex subclouds (in the maxilla) or even significantly broader than apex subclouds (in the mandible).

We suggest that the "angular ordering" (i.e., along θ) of crown $\mathcal{L}$-arches is due to the fact that crowns have finite size and are in contact: Thus, a crown landmark can not come arbitrarily close to another. Conversely, since interproximal contact points for apexes either do not exist or have a lesser extent than crown contact points, apexes result to be more free to organize within the jaw (eventually leading to what we might call "apex crowding"). The crown angular ordering (relative to apexes) is more pronounced

for latero-posterior teeth (smaller F-ratios in Fig. 6), which exhibit larger interproximal surfaces, than anterior teeth, whose interproximal contacts are nearly point-like. Along nearly BL (ρ) direction instead interproximal contacts are not present, both for apexes and crowns. Consistently, BL crown cloud size may even be larger than corresponding apex cloud size.

θ		l5	l4	l3	l2	l1	r1	r2	r3	r4	r5
Maxilla	$S_c[^o]$	1.5	2.0	1.7	1.5	1.7	2.0	2.2	2.3	2.1	1.6
	$S_a[^o]$	3.6	3.6	3.2	2.8	2.2	2.2	3.2	2.8	3.3	3.9
	S_c^2/S_a^2	.17	.32	.26	.29	.59	.82	.47	.68	.40	.17
	p	0	.003	0	.002	*.165*	*.599*	*.051*	*.305*	.018	0
Mandible	$S_c[^o]$	1.7	2.2	1.7	1.6	1.5	1.5	2.2	3.5	2.2	1.8
	$S_a[^o]$	2.9	3.7	3.1	3.0	2.2	1.8	2.7	4.0	4.1	3.5
	S_c^2/S_a^2	.36	.36	.30	.29	.45	.72	.62	.78	.29	.27
	p	.002	.002	0	0	.015	*.307*	*.150*	*.449*	0	0

Table 4: *Statistical summary table for θ direction. For each tooth, the standard deviation S of the subcloud along θ for both crown and apex $\mathcal{L}$-arch; the $S_c^2/S_a^2 = F$ ratio and the p-value for the $F = 1$ hypothesis are given. The $F = 1$ hypothesis can be accepted for $p > .050$. In such case, the p-value is printed in italics. The "0" figure is used for p-values $<$ 1.e-3.*

ρ		l5	l4	l3	l2	l1	r1	r2	r3	r4	r5
Maxilla	S_c	.016	.028	.046	.052	.066	.065	.049	.042	.023	.016
	S_a	.023	.03	.039	.045	.054	.056	.047	.041	.026	.021
	S_c^2/S_a^2	.45	.89	1.37	1.35	1.49	1.35	1.08	1.08	.81	.55
	p	.037	*.750*	*.406*	*.437*	*.297*	*.428*	*.836*	*.846*	*.577*	*.120*
Mandible	S_c	.018	.029	.044	.053	.055	.053	.05	.057	.033	.015
	S_a	.020	.023	.030	.030	.032	.032	.030	.026	.020	.015
	S_c^2/S_a^2	.79	1.53	2.10	3.25	2.91	2.73	2.76	4.65	2.6	1.10
	p	*.467*	*.191*	.025	0	.001	.003	.002	0	.004	*.777*

Table 5: *Statistical summary table for ρ direction. For each tooth, the standard deviation S of the subcloud along ρ for both crown and apex $\mathcal{L}$-arch; the $S_c^2/S_a^2 = F$ ratio and the p-value for the $F = 1$ hypothesis are given. The $F = 1$ hypothesis can be accepted for $p > .050$. In such case, the p-value is printed in italics. The "0" figure is used for p-values $<$ 1.e-3.*

3.2 $\mathcal{L}$-arch shape

We have found that $\mathcal{L}$-arch shape is most easily described in the polar representation of Fig. 5. The simple harmonic expansion given by Eq. (5) provides a good fitting of the data in all $\mathcal{L}$-arches: all 4 fits pass the χ^2-test with p-value = 1. Corresponding fit parameters ρ_1, ρ_3 are listed in Tab. 6. The fit functions do not always pass by the tooth average positions. A more complex fit function, containing higher harmonics which still satisfy the boundary conditions expressed in Sect. (2.2.4), could better fit the data. However, given the relatively small number (10) of datapoints to be fitted, it would be hard to obtain more than 2 independent fit parameters with good accuracy. Thus, the proposed function Eq. (5) represents a fair compromise between fit quality and simplicity. Furthermore, both

	crown_up	apex_up	crown_dn	apex_dn
ρ_1	.13±.02	.07±.02	.08±.02	-.06±.01
ρ_3	.07±.01	.03±.01	.06±.01	.03±.01

Table 6: *Summary table of fit results. All fits of Eq. (5) to the mean tooth positions of Fig. 5 pass the χ^2-test with p-value=1. The parameter uncertainties stem from the fitting procedure, which accounts for statistical errors along both θ and ρ axes (ODRPACK95 routine). The ρ_1 and ρ_3 parameters are expressed in units of the distance between first molars.*

fit parameters ρ_1 and ρ_3 have a simple geometrical meaning, as explaiin Sect. (2.2.4). It should also be stressed that our fit function i) applies to all four $\mathcal{L}$-arches, despite their qualitative differences, and ii) depends on two free parameters only, ρ_1 and ρ_3. The quality of the fits is unchanged by their back transformation to rectangular coordinates using the inverse of Eq. (2) (see Fig. 4). Furthermore, the rectangular coordinate representation exalts the flexibility of the fit function Eq. (5): Curves of the very same family are able to describe shapes as much different as the nearly semicircular mandible apex $\mathcal{L}$-arch and the not trivial, curvature changing maxilla crown $\mathcal{L}$-arch. Previous attempts to describe such shape resorted to more complex fit functions, varying from catenary curves [8], polynomials of not integral order such as the β-function [2], high order polynomials (up to 7 free parameters) [8] long harmonic expansions (up to 24 harmonics) [6], up to mixed models in which a conic section arch is connected to straight lines [3] or to a polynomial function [12]. In our view, such complexity is mainly due to the fact that the cartesian frame is not the most convenient system for describing the geometry of dental arches. A polar frame seems to be more appropriate for gently following BL and MD directions.

4 Discussion

In this section we discuss some critical points of our work.

1) The choice of the landmark definition. The $\mathcal{L}$-arch structure depends on this choice, which is not unique. Furthermore, universally accepted guidelines for the landmark placement of tooth landmarks are not found in the literature. Our criteria in the definition of crown and apex landmark position were simplicity and reproducibility. Thus, following alternative definitions of crown landmark were ruled out:

   - Points on the vestibular surface. These are strongly affected by the choice of the assial section because of tooth tilting;
   - The center of the tooth occlusal surface. This is strongly affected by the choice of the assial section because of tooth tilting and tooth shape;
   - Cuspids. They can be hardly recognized in CT images due to overlap with cupids of the antagonist dental arch (in occlusion).

   In addition, we note that, for the sake of internal consistence of the method, it is of paramount importance that landmark placement is done by the same operator for all patient data (as we did).

2) It might be asked if and how the actual choice of the fixed points affects subsequent results of our investigation. In Fig. 5 and, more explicitly, in Tab. 4 it is seen that cloud size along nearly MD (θ) direction does not change significantly among teeth of

a given $\mathcal{L}$-arch, both for crown and apex $\mathcal{L}$-arches (see S_c, S_a standard deviations). Conversely, from Tab. 5 it is seen that cloud size along nearly BL (ρ) direction increases from molars to central incisors, both for crown and apex $\mathcal{L}$-arches. Thus, the actual choice of the fixed points at the first molar location primarily affects cloud size along nearly BL direction (ρ). However, our main statement concerns the ratio of crown to apex cloud variances along a nearly MD direction (θ). Furthermore, if any residual systematic effect due to the fixed points is still present in the cloud sizes along θ, it is reasonably removed when considering the S_c^2/S_a^2 ratio of cloud variances between $\mathcal{L}$-arches belonging the same dental arch. As a consequence, we believe that the observed trend in the $F-$ratio along θ as seen in Fig. 6 is real and is not an artifact of the used method for coordinate standardization.

3) Another important point is the polar transformation Eq. (2), which allows exploring $\mathcal{L}$-arch data in a more natural reference frame. The motivation for operating such a transformation was to be able to gently follow the geometry of the dental arches. A frame was seeked, into which the BL and MD directions could be recognized more easily than in the rectangular Cartesian frame. If for example the $\mathcal{L}$-arches were elliptic in shape, ideally such a frame would be represented by an elliptic coordinate system. However, such a hypothetical system would present the disadvantage of depending on parameters (locations of ellipse's foci) which eventually are function of the data. On the other hand, the polar transformation Eq. (2), not depending on external parameters, is remarkably simple. Though its axes coincide exactly with BL and MD directions in a limiting case only (i.e., semicircular $\mathcal{L}$-arch), the polar frame highlights the most important features of the $\mathcal{L}$-arch subcloud structure (Fig. 5) and allows a simple two-parameter fitting of $\mathcal{L}$-arch shape, Eq. (5).

5 Conclusions

In this paper we presented a method based on CT images for investigating dental positions, treating crown and radicular apex data on the same footing.

The main steps of the method can be summarized as:

- selection of CT assial sections;
- definition of landmarks;
- standardization of landmark coordinates (Eq. (1));
- transformation into polar coordinates (Eq. (2));
- analysis of subcloud size;
- analysis of mean shape of the landmark arches (Eq. (5)).

The standardization of landmark coordinates allowed us to compare landmarks from different patients. It revealed that landmarks relative to a given tooth cluster around a mean position ("subcloud structure", see Fig. 4). Such clustering tends to be angularly more definite for crown than apex landmarks.

Furthermore, the standardized data prove that the system of polar coordinates is a powerful tool for the investigation of dental positions, due to its ability to (approximately) follow the BL and the MD directions. Within the polar frame, it appears more clearly

that subclouds are elongated along the BL direction (Fig. 5). A central result of our investigations is that, in these regards, there is a statistically significant distinction between crown and apex: A given crown subclouds indeed is located at an angular position which is better defined than the corresponding apex angular position (Fig. 6 and Tab. 4, Tab. 5). This holds for both maxilla and mandible.

The polar frame appears also to be the natural choice for the description of the mean shape of what we called "landmark arches"(Sect. (2.2)): We were able to provide a simple two-parameter fitting model, Eq. (5), which applies to both crown and apex data, both in the maxilla and the mandible case. Despite its simplicity, such model provides good fits of the mean $\mathcal{L}$-arches. While mean apical $\mathcal{L}$-arches are nearly hemicircular in shape, crown $\mathcal{L}$-arches have a composite shape, which is round in the vicinity of anterior teeth and close to a straight line for latero-posterior teeth.

The observation that (most) crown subcloud are significantly narrower than apex subcloud along the angular direction might be due to the fact that apexes do not have interproximal contact points while crowns do have. The interproximal contacts indeed limit the variability of crown positioning along MD direction. Furthermore, the interproximal contacts are wider for latero-posterior than anterior teeth and this is consistent with our statistical results of Fig. 6, indicating a smaller ratio of crown to apex subcloud width for latero-posterior than anterior teeth. In the radial or nearly BL direction interproximal contacts are absent by definition. Consistently, along this direction crown variability does not exhibit any trend with respect to apex variability. Depending on the dental arch, the variability of radial crown position can be comparable or even larger than the variability at apex level.

Mean $\mathcal{L}$-arch shape too is consistent with the picture according to which interproximal contacts are like "hinges" in the dental arch. If such hinges have a finite extension in MD direction, torsion between adjacent teeth is strongly limited. This is the case indeed for crowns of latero-posterior teeth. Conversely, where hinges have a more limited area, adjacent teeth can adjust into a circular arch (anterior crowns and both anterior and latero-posterior apexes).

6 Acknowledgements

The following private centers in Italy are kindly acknowledged for providing CT data: Quarta Colosso radiologic center in Lecce; Dr. Carlo Perissinotto's private practice in Treviso; Pasta radiologic center in Parma; Apollonia radiologic center in Lecce.

References

[1] E. A. BeGole and R. C. Lyew. A new method for analyzing change in dental arch form. *Am J Orthod Dentofacial Orthop*, 113:394–401, 1998.

[2] S. Braun, W. P. Hnat, D. E. Fender, and H. L. Legan. The form of the human dental arch. *Angle Orthod*, 68:29–36, 1998.

[3] V. F. Ferrario, C. Sforza, A. Miani Jr, and G. Tartaglia. Mathematical definition of the shape of dental arches in human permanent healthy dentitions. *European Journal of Orthodontics*, 16:287–294, 1994.

[4] C. A. Hawley. Determination of the normal arch, and its application of orthodontia. *The Dental Cosmos*, 47:541–552, 1905.

[5] Bookstein F. L. *Morphometrics Tools for Landmark Data*. Cambridge University Press, 1991.

[6] P. E. Lestrel, O. Takahashi, and E. Kanazawa. A quantitative approach for measuring crowding in the dental arch: Fourier descriptors. *Am J Orthod Dentofacial Orthop*, 125:716–725, 2004.

[7] A. Nakajima, G. T. Sameshima, Y. Arai, Y. Homme, N. Shimizu, and H. Dougherty Sr. Two- and three-dimensional orthodontic imaging using limited cone beam computed tomography. *Angle Orthod*, 75:895–903, 2005.

[8] S. H. Pepe. Polynomial and catenary curve fits to human dental arches. *J Dent Res*, 54:1124–1132, 1975.

[9] V. Ronay, R. M. Miner, L. A. Will, and K. Arai. Mandibular arch form: The relationship between dental and basal anatomy. *Am J Orthod Dentofacial Orthop*, 134:430–438, 2008.

[10] P. D. Sampson. Dental arch shape: A statistical analysis using conic sections. *Am J Orthod*, 79:535–548, 1981.

[11] K. Vargervick. Morphologic evidence of muscle influence on dental arch width. *Am J Orthod*, 76:21–28, 1979.

[12] H. Wellens. Applicability of mathematical curve-fitting procedures to late mixed dentition patients with crowding: A clinical-experimental evaluation. *Am J Orthod Dentofacial Orthop*, 131:160.e17–160.e25, 2007.

[13] L. W. White. Individualized ideal arches. *J Clin Orthod*, 12:779–787, 1978.